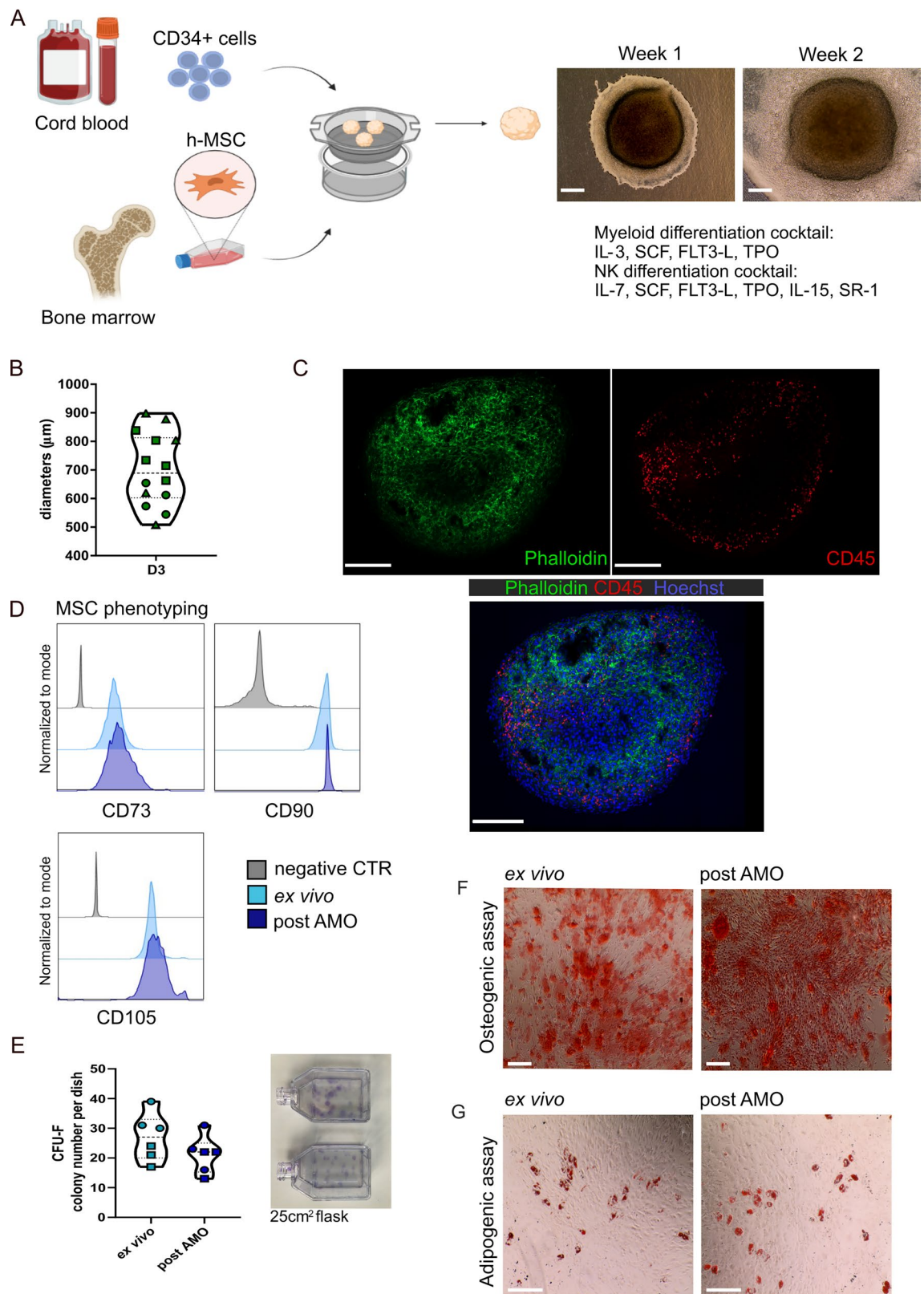# scientific reports

OPEN

Modeling mesenchymal stromal cell support to hematopoiesis within a novel 3D artificial marrow organoid system

Bérénice Schell[1,2,6], Lin-Pierre Zhao[1,2,3,6], Inés M'Sibih[1,2], Maria Kalogeraki[1,2], Camille Kergaravat[1,2], Emilie Lereclus[1,2,4], Pierre Fenaux[1,2,3], Lionel Adès[1,2,3], Antoine Toubert[1,2,5], Marion Espéli[1,2], Karl Balabanian[1,2], Emmanuel Clave[1,2], Nicolas Dulphy[1,2,5,7✉] & Valeria Bisio[1,2,7✉]

The human bone marrow (BM) microenvironment involves hematopoietic and non-hematopoietic cell subsets organized in a complex architecture. Tremendous efforts have been made to model it in order to analyze normal or pathological hematopoiesis and its stromal counterpart. Herein, we report an original, fully-human *in vitro* 3D model of the BM microenvironment dedicated to study interactions taking place between mesenchymal stromal cells (MSC) and hematopoietic stem and progenitor cells (HSPC) during the hematopoietic differentiation. This fully-human Artificial Marrow Organoid (AMO) model is highly efficient to recapitulate MSC support to myeloid differentiation and NK cell development from the immature CD34 + HSPCs to the most terminally differentiated CD15 + polymorphonuclear neutrophils, CD64 + monocytes or NKG2A-KIR2D + CD57 + NK subset. Lastly, our model is suitable for evaluating anti-leukemic NK cell function in presence of therapeutic agents. Overall, the AMO is a versatile, low cost and simple model able to recapitulate normal hematopoiesis and allowing more physiological drug testing by taking into account both immune and non-immune BM microenvironment interactions.

Reproducible and reliable fully-humanized models are still needed to study the complex cellular interplay taking place within bone marrow (BM) hematopoietic niches. Ideally, such a model should use primary cells and replicate the local BM microenvironment (BMM), including a functional immune system. Additionally, this model should be user-friendly, fast, reproducible, and cost-effective. A wide range of in vivo models have been developed but all face major drawbacks in terms of transferability to human (no immunological context), poor engraftment of hematopoietic stem and progenitor cells (HSPCs) into recipient mice and high technical complexity[1,2]. Therefore, 2D *in vitro* models are still widely used, due to their relative simplicity, cheapness and reproducibility. However, they miss the spatial organization and biomechanical forces of the BMM, crucial for the cellular fate. To overcome this point, there has been a surge of interest for the development of 3D models[3–5] that so far do not meet simultaneously the requirements of user-friendliness, reproducibility, low cost and system versatility. To bridge this technological gap, we developed a novel approach for generating BM organoids that exhibit *in vivo*-like functional hematopoietic capabilities as the capacity to derive terminally differentiating myeloid or lymphoid lineages from progenitor cells. The two differentiation programs are complex and highly regulated processes that give rise to fully committed cells[6,7]. Myeloid differentiation is a particularly intricate and tightly controlled process that produces granulocytes, erythrocytes, and monocytes, the last being able to further mature into macrophages and dendritic cells[8,9]. Inside the myeloid lineage, granulocytes represented a particular challenge to be generated in vitro, as *ex vivo* isolated cells appear difficult to use in experiments, due to their short lifespan[10]. Concerning the lymphoid lineage, it comprises various types of lymphocytes, including T,

B, and natural killer (NK) cells[7,11]. The NK cells are of particular interest as they currently constitute a major area of innovation in the field of immunotherapy[12] due to their spontaneous capacity to produce cytokines (IFN-γ/TNF-α), cytolytic proteins (perforin/granzymes) and kill target cells, NK lymphocytes were described for decades as very potent anti-tumor effector cells[13,14]. Consequently, many attempts have been made to generate NK cells in vitro, especially for adoptive immunotherapy, with often disappointing results as for the expression of terminal differentiation KIR molecules[15–17]. Hence, a versatile model able to produce both myeloid and NK cells seemed of particular interest for the scientific community.

◄**Fig. 1**. Artificial Marrow Organoid (AMO) formation and observation. AMO can be formed by concentrating h-MSCs and other cell types and depositing a drop of cell concentrate in a membrane placed over cell-culture medium. (**A**) CD34 + hematopoietic stem and progenitor cells isolated from cord blood were differentiated into myeloid and NK cells in AMO using an appropriate cocktail of cytokines. Direct optical microscopic observations of AMO with CD34 + HSPCs after 7 and 14 days of culture are shown. Scale bar 100 μm. (**B**) Violin plot of the AMO diameters on day 3 of culture ($n = 14$, 3 different h-MSCs are indicated with different shape: MSC#1 square, MSC#2 triangle and MSC#3 circle. $N = 5$, 5 and 4 replicates respectively). Data are represented as mean ± SD. (**C**) Analysis of a representative whole mount organoid stained with Hoechst (nuclei, blue), Phalloidin-FITC (stromal counterpart, green) and CD45-AF647 (hematopoietic counterpart cell membrane, red). Scale bar 100 μm. One representative experiment of three is presented. (**D-G**) Characterization of FACS-sorted h-MSCs after 2 weeks of AMO co-culture, compared to paired *ex vivo* h-MSCs. (**D**) Histograms showing expression of 3 mesenchymal lineage markers CD73, CD90 and CD105 assessed by flow cytometry compared to unstained cells (negative control, in grey). H-MSCs are gated on forward scatter. One representative experiment of three is presented. (**E**) Colony Forming Unit Fibroblast (CFU-F) assay of h-MSCs after crystal violet staining. The 2 different h-MSCs used are indicated with different shape: MSC#1 square, MSC#2 circle. A triplicate for each h-MSC has been performed. (**F**) Osteogenic differentiation of h-MSCs stained with red alizarin. Scale bar 200 μm. (**G**) Adipogenic differentiation of h-MSCs observed after oil red staining. Scale bar 50 μm. One representative experiment of three is presented.

Herein, we describe an easy-to-access, reliable and reproducible self-organizing *in vitro* 3D model for studying progenitor and mature hematopoietic cells in the frame of their physical crosstalk with the human mesenchymal BM stroma. Importantly, we also provided proof-of-concept for the use of this system for drug screening. We, thus, believe that this artificial marrow organoid (AMO) holds great promise as a preclinical model for pharmacologic assays and toxicity studies of novel drugs in a BM mimicking 3D environment.

Results

The artifical marrow organoid is a self-organizing reproducible culture model that preserves the MSC properties

The Artificial Marrow Organoid (AMO), is based on the *Seet et al.* model[18] in which we substituted the murine stromal cell line MS5-hDLL1 with *ex vivo* expanded human primary BM MSCs (h-MSCs). To promote hematological differentiation process, h-MSCs ($N = 8-15 \times 10^4$), isolated by cell-to-plastic adhesion of BM samples from healthy donors ($n = 4$, see material and methods for more details) hip replacement surgery, were expanded and co-cultured with a small number of sorted CD34 + HSPCs ($N = 6-7.5 \times 10^3$) in presence of a specific cocktail of cytokines (Fig. 1A). The organoids assembled into a spherical shape (Fig. 1A) with a median diameter of 689 μm (range: 508 to 898 μm) after 3 days of culture (Fig. 1B). Confocal microscopy revealed CD45 + hematopoietic cells (in red) embedded into a network of stromal cells (in green, Fig. 1C). Compared to the corresponding *ex vivo*-expanded stromal cells, the h-MSCs sorted from AMO after two weeks of culture retained the same characteristics in terms of mesenchymal-lineage markers (CD73 + CD90 + CD105+; Fig. 1D), plastic adherence ability, clonogenic capacity (Fig. 1E), and osteogenic and adipogenic differentiation potential (Fig. 1F-G). Importantly, this self-organizing model does not require external support, such as hydrogel or collagen matrix, in contrast to other previously published systems[5,19].

The AMO model enhances HSPCs maintenance and myeloid differentiation compared to standard 2D MSC/HSPC co-culture

Taking advantage of the simplicity and high reproducibility of our model, we tested whether it could support myeloid-cell development starting from freshly isolated human cord blood CD34 + HSPCs. May Grunwald Giemsa-stained cytospins of myeloid cells after 3 weeks of culture showed characteristic morphology of the myeloid progenitor and mature myeloid cells (monocytic and granulocytic cells) covering all the stages of the myeloid differentiation (Fig. 2A, black and red arrow respectively). In line with this observation, and given that most immature CD34 + cell population exhibit weak CD45 expression while cells committed to the myeloid cell line progressively gained CD45 antigen expression[20] we performed confocal microscopy analysis to evaluate the progressive maturation of the myeloid subsets. Our results showed a significant 1.7-fold increase of the CD45 expression over time (Mean Intensity CD45-AF647: 4251,7 and 7265,8 at day 7 and day 21 respectively, p-value of paired t test < 0.001, Fig. 2B-C). Moreover, we analyzed the spatial localization of the CD45 + cells in the AMO, observing a scattered distribution with a tendency for localization at the edges more than in the center of the organoid (Fig. 2D, p-value of paired t test < 0.0001). Next, we quantified more precisely the myeloid differentiation program by flow cytometry. Myeloid progenitors were distinguished from their erythroid counterparts, by expression of either CD71 or CD235a. After lymphocyte elimination, mature myeloid cells were defined as CD15 + for polymorphonuclear neutrophils (PMN) or CD33 + CD64 + for monocytes (gating strategy in Fig. 3A). Based on the expression of these specific cell surface markers, the myeloid differentiation was tracked from promyelocytes to myelocytes and beyond. Mature cells were identified in the AMO from week 1 to week 3 (Fig. 3B, Supplemental Fig. 1 A). We observed a general decrease of the immature cell marker, CD34, together with an increase in all mature myeloid markers (CD33, CD13, CD45, CD64, CD15, CD11b) over time.

Interestingly the AMO showed a persistence of CD34 + HSPCs for the 21 days of culture compared to a classical 2D co-culture model composed by the same h-MSC and CD34 + cells (Mann Whitney test p-values: 0.03, 0.02 and 0.005 for day 7, day 14 and day 21 respectively, Fig. 3C). The maintenance of immature progenitors
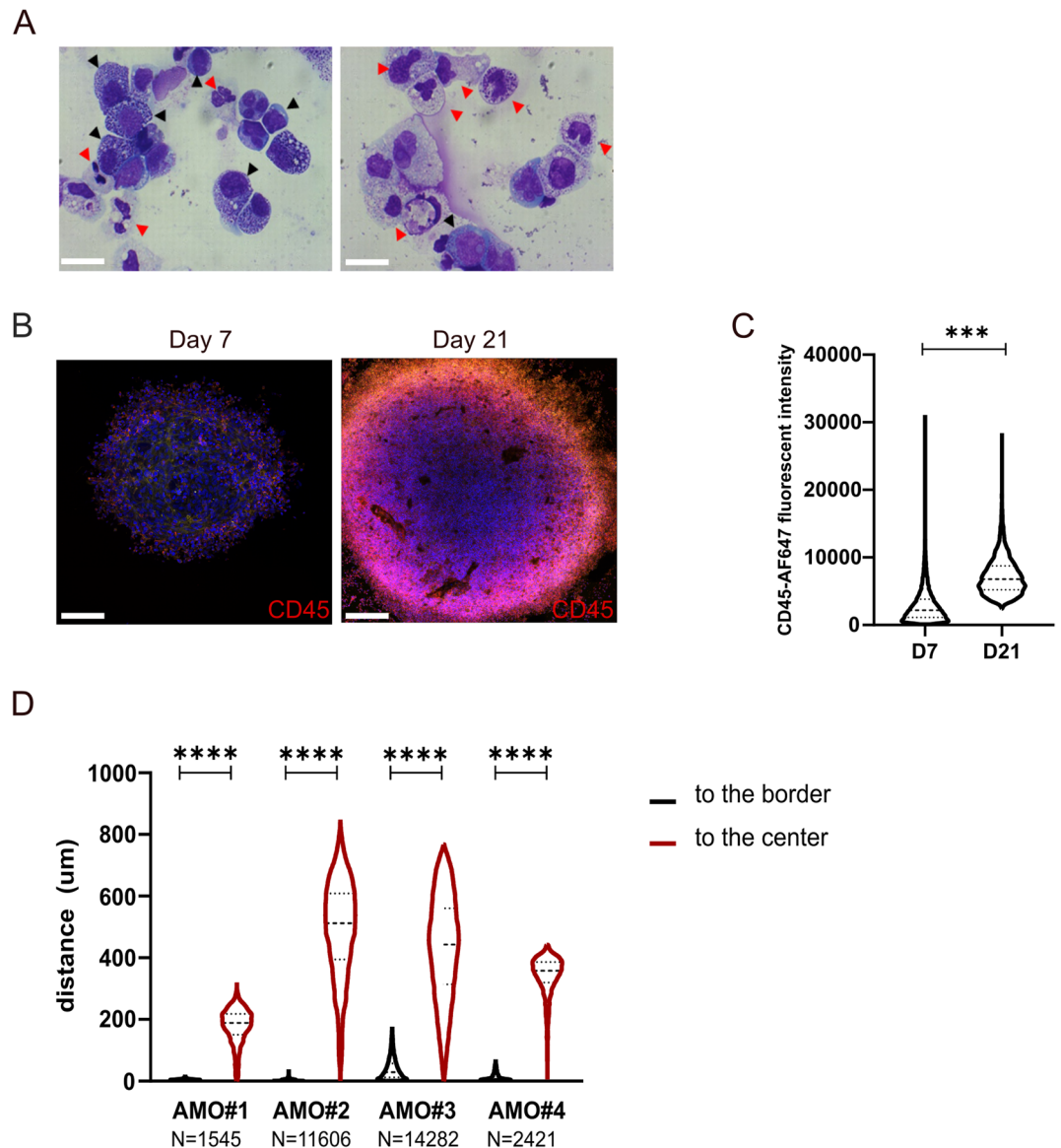
Fig. 2. Myeloid cell commitment from CD34 + HSPCs in AMO. (**A**) Morphological evaluation of one representative myeloid cell differentiation at 21 days observed after MGG staining of AMO cell cytospin. One representative experiment out of three is presented. Black arrow: immature myeloid cells. Red arrow: mature myeloid cells. Scale bar 60 μm (**B-C**) Analysis at day 7 (left) and 21 (right) of a representative whole mount organoid stained with Hoechst (nuclei, blue) and CD45-AF647 (hematopoietic counterpart cell membrane, red). (**B**) Picture of one representative experiment out of three is presented. Scale bar 100 μm. (**C**) Quantification of the CD45 intensity ($N = 15808$ and 11237 cells, at day 7 and day 21 respectively) from 3 different experiments; p-value of paired t test < 0.001. Data are represented as mean ± SD. (**D**) Spatial cells´ distance of CD45 + cells to the organoid border (black) or center (red) at day 7 for 4 independent AMO numerated from 1 to 4 ($N = 1545$, 11606, 14282, 2421 cells analyzed for independent organoid). Data are represented as mean ± SD.

was reminiscent of our previous results showing the presence of myeloblasts and immature granulocytic cells visible by morphological examination after 3 weeks of culture (Fig. 2A).

To examine whether the AMO-persistent HSPCs retained stemness capacities, we performed colony-forming unit (CFU) assays after two weeks of culture with the myeloid differentiation protocol. FACS-sorted AMO-cultured HSPCs gave rise to granulocyte-macrophage progenitor cells (CFU-GM) and also to a minority of multipotent progenitor cells, including granulocyte, erythroid, macrophage, and megakaryocyte progenitors (CFU-GEMM) (Fig. 3D). Additionally, a secondary passage in organoid structures was performed with a portion of the HSPCs sorted from the primary AMO. As shown in Fig. 3E, these cells retained the ability to differentiate into monocytes and polymorphonuclear cells after additional two weeks of culture in the myeloid differentiation

cytokines cocktail. These results provide evidence of the multilineage differentiation potential and functionality of the HSPCs present in the AMO.

Secondly, compared to the 2D culture, the AMO model showed an increased percentage of PMNs at day 21 (Mann Whitney test p-value: 0.007, Fig. 3C) and a decreased percentage of monocytes at all time points (Mann Whitney test p-values: 0.03, < 0.001 and 0.002 for day 7, day 14 and day 21 respectively, Fig. 3C), suggesting that the 3D organization of the model favored granulocytic over monocytic lineage differentiation, contrary to the 2D co-culture. This was confirmed also by light microscopy analysis on flow sorted CD45 + and MGG stained cells showing an increased PMN in the AMO compared to the 2D system (Fig. 3F). Flow-cytometric analysis validated the elevated expression of the myeloperoxidase (MPO) only in the PMN cells, while the monocytes exhibited typical intermediate to low MPO levels (Fig. 3G). Only a few B (CD19 + CD7-; 0,03%, 0,007% and 0,013% at day 7, day 14 and day 21 in the AMO condition) and NK lymphoid cells (CD19-CD3-CD7 + CD56low or CD56high; 0,7% 1,04% and 2,43% at day 7, day 14 and day 21 in the AMO condition) were identified with this cocktail of cytokines, while no T cells (CD19-CD7 + CD3+) have been found, underlining the specificity of our protocol for the development of myeloid subsets (Supplemental Fig. 1B-C).

These findings indicate that the AMO model promotes maturation of monocytes and neutrophils, providing a model to study the emergence of myeloid cells and in particular of granulopoiesis in a fully human context.
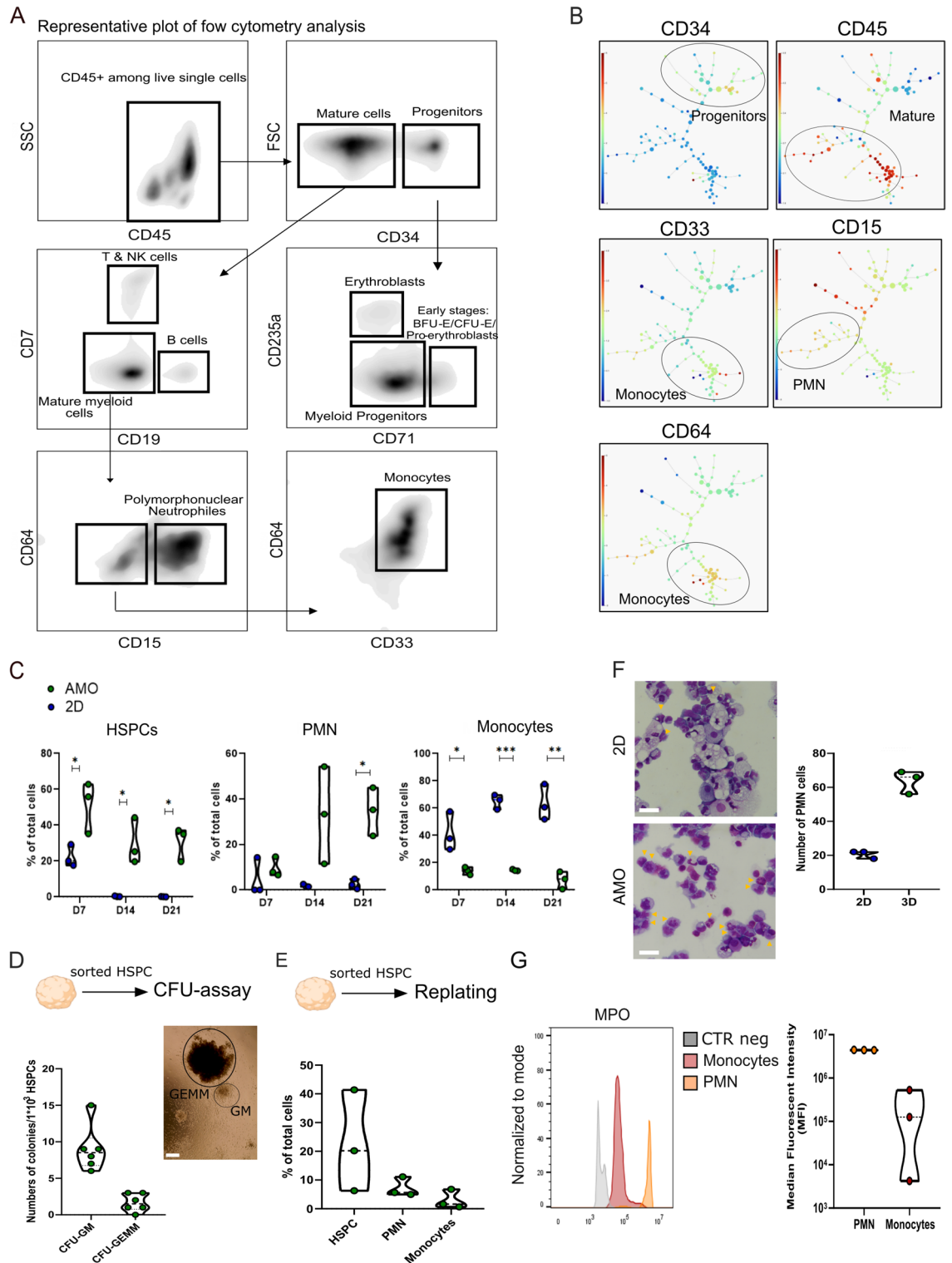
The AMO model serves as an efficient platform for NK cell lymphopoiesis

We next analyzed the innate lymphoid differentiation potential of the AMO model. Starting from freshly isolated human cord blood CD34 + HSPCs, with a specific cocktail of cytokines (Fig. 1A), the NK-cell commitment was completed within 1 to 4 weeks and up to 2×10^5 total NK cells were generated from one single organoid. Flow-cytometry analysis, using an appropriate gating strategy (Fig. 4A), based on previously described NK cell maturation stages[21] (Supplemental Fig. 2 A) and pseudotime trajectories (Fig. 4B), were used to visualize the progression of NK cell development from HSPCs to the different NK maturation stages. Since week 2, the AMO supported efficient NK cell lineage commitment and recapitulated the full NK cell differentiation starting from HSCs (stage 1) to the CD34 + CD10 + CD45RA + common lymphoid progenitor (CLP, stage 2), Lin-CD56- (stage 3), Lin-CD56 + CD16- (stage 4), Lin-CD56 + CD16+ (stage 5) and finally Lin-CD56 + CD16 + CD57+ (stage 6) NK cells (Fig. 4A-B). Pseudotime analysis objectified this maturation trajectory from CD34 + HSC and CLP with a progressive acquisition of CD56 + and NK markers such as CD94 and NKp46, acquired simultaneously during stage 3, and then NKp80 acquired at stage 4 (Fig. 3B and Supplemental Fig. 2B). Very few immature T (CD7 + CD56-) and mature B cells (CD19+) originated from HSPC under this differentiating protocol. The supervised population gating showed that, by week 2, the majority of cells have engaged into NK cell differentiation (stage 3: 47.9% and stage 4: 41.3%) while only few HSC (0.3%) and CLP (2.1%) were still present (Fig. 4C). These immature cells completely disappeared by week 4 when the majority of cells belong to stage 4 (77.2%) with an increase of cells in stage 5 (13.5%). As expected, the NK stage 5 was characterized by the expression of activating (NKp30, DNAM-1) and inhibitory receptors (NKG2A and KIR molecules) crucial for NK cell functionality (Fig. 4D). By contrast to *in vitro* 2D co-culture[16,17] the AMO is not only able to support NK cell differentiation but also to reproduce the natural NK cell heterogeneity (according to the expression of NKG2A and KIR molecules), until the late terminally differentiated NKG2A-KIR + CD57 + NK-cell subset (stage 6) (Fig. 4C). Importantly, NK cells produced after AMO-based differentiation were polyfunctional, as demonstrated by their capacity to degranulate cytolytic granules and produce IFN-γ and TNF-α (Fig. 4E, Supplemental Table 1). In fact, the proportion of NK cells with monofunction, bifunction and trifunction significantly increased after stimulation by the NK sensitive HLA-Class I-negative K562 cell line or PMA and ionomycin. Remarkably, the cytotoxic capacity against K562 cells, albeit variable, tended to be comparable than that of mature NK cells sorted directly from peripheral blood ($N = 3$, Supplemental Fig. 2 C), thus confirming that this model allowed the production of fully functional and mature NK cells with a high efficiency.

AMO as a tool to investigate drug-induced modulation of NK cell functions in an MSC-based microenvironment

Finally, we explored whether the AMO may be suitable to test drug *ex vivo*. For this purpose, mature NK-cells isolated from PBMC were co-cultured with h-MSCs in the AMO model. Histological analysis showed the infiltration of isolated NK-cells (CellTrace Yellow, in yellow and CD45 in red), surrounded by h-MSC (CD271, in green) within the 3D structure (Fig. 5A). After one week of culture, the NK cells maintained the expression of lineage-specific markers (CD16 and CD56; Fig. 5B), as well as their capacity to proliferate and kill cancer cells, specifically the K562 cell line (Fig. 5C, left panel). Proliferation was further assessed according to the expression of the Ki67 marker (Fig. 5C, right panel).

We next evaluated the drug permeability of our model by incubating for 2 hours the AMO with the doxorubicin (DOXO), with known autofluorescence property[22]. The yellow autofluorescence signal associated with the DOXO was quantified by confocal imaging and compared to the signal with the DMSO alone. This analysis revealed a 1.9-fold increase in fluorescence intensity under DOXO conditions, indicating an efficient drug delivery throughout the entire 3D structure (Fig. 5D, Wilcoxon test p-value < 0,0001). This result prompted us to test treatments with the hypomethylating agents azacytidine (AZA) and decitabine (5-aza-2'-deoxycytidine, DAC), commonly used to treat high-risk MDS (Myelodysplastic Syndromes) and AML (Acute myeloid leukemia) patients, and known to increase NK cell cytotoxic functionality[17,23,24]. After 3 days of culture in AMO in presence of AZA or DAC, we observed an increased NK cytotoxicity against the NK sensitive K562 cell line upon treatment, confirming the drug efficacy within the AMO system, particularly following DAC treatment (Fig. 5E, Mann Whitney test p-values < 0,05). Thus, the AMO system exhibited a significant potential as a BM-mimicking platform for *in vitro* immunomodulatory drug testing.

A — Representative plot of flow cytometry analysis

B — CD34, CD45, CD33, CD15, CD64

C — AMO / 2D: HSPCs, PMN, Monocytes

D — sorted HSPC → CFU-assay

E — sorted HSPC → Replating

F — 2D / AMO; Number of PMN cells

G — MPO; Median Fluorescent Intensity (MFI)

Discussion

The BM is an essential tissue responsible for the production of blood cells through a process known as hematopoiesis. This dynamic environment is home to HSCs, which give rise to various blood cell lineages, including NK and myeloid cells. Understanding the cell ontogenesis in the BM is mandatory for deciphering the pathophysiology of various hematological disorders, including MDS and leukemia[25,26]. Research in this area can lead to the identification of therapeutic targets and the development of treatments aimed at modulating the BM microenvironment to enhance immune surveillance and inhibit tumor progression. Despite significant successes in treating solid tumors and some hematological malignancies, immunotherapies are still inefficient to treat AML and related diseases such as MDS. Several issues could be raised to explain these frustrating results, including the immune selection of resistant clones, absence or irrelevance of the expression of immune checkpoints or their ligands, or the generation at the neighborhood of the leukemic niche of an immunosuppressive
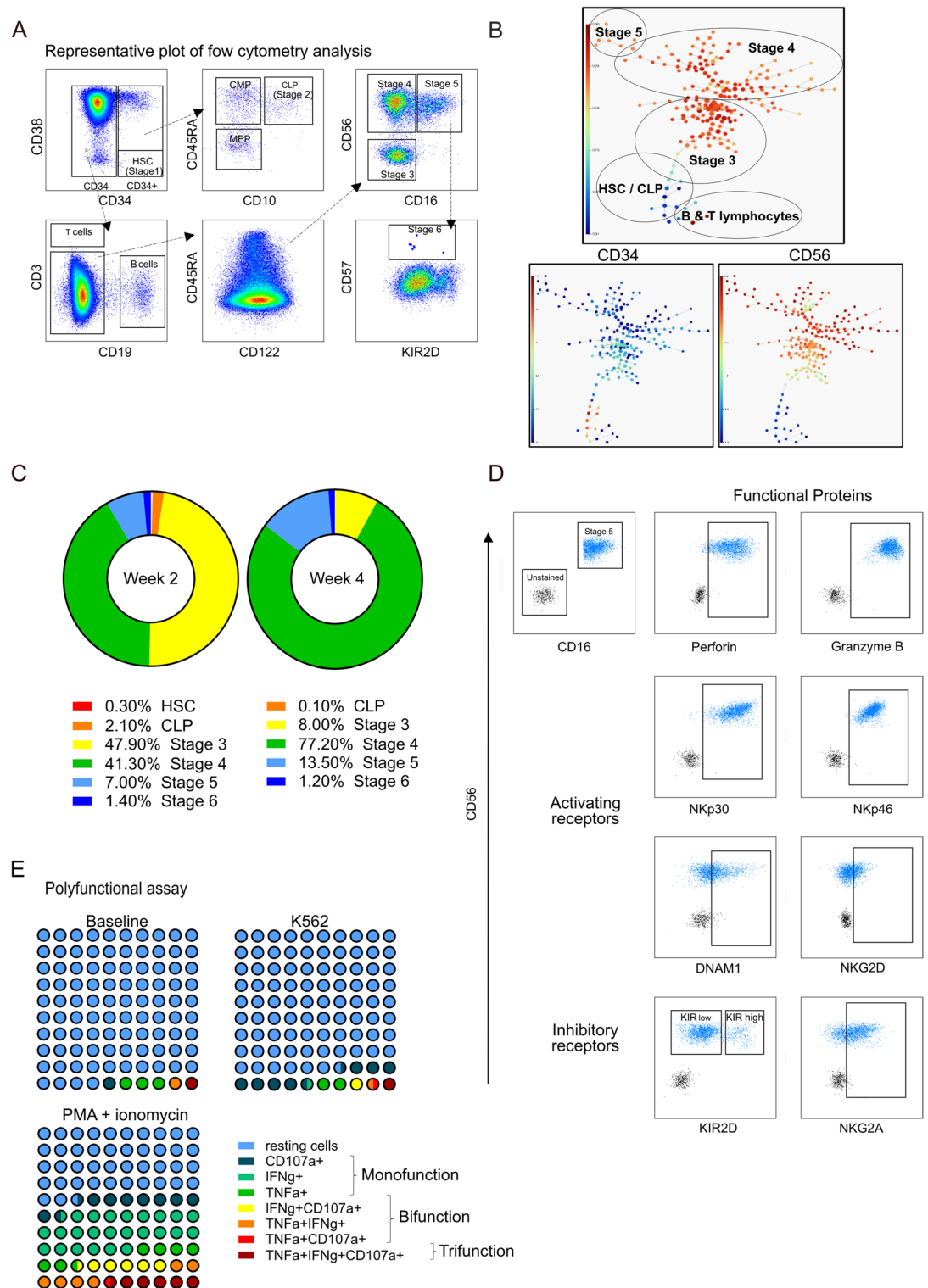
◀ **Fig. 3**. Myeloid cell characterization within the AMO. (**A**) Gatting strategy for the myeloid differentiation analysis on dissociated AMO: myeloid progenitors (CD34+, CD71- CD235a-), PMNs (CD15+) and monocytes (CD33 + CD64+). Plots at three weeks of differentiation. (**B**) Tree representation of FLOWSOM clustering colored by pseudotime calculated using trajectory analysis with Wishbone algorithm of myeloid cell differentiation taking CD34 + CD38- HSC population as starting cell type. The size of nodes is proportional to the number of cells in the given cluster. Calculation and figure were made with the OMIQ software (https://www.omiq.ai). The differentiation stages have been manually added to the figure based on the expression of main lineage markers. The same FLOWSOM tree is represented from the left panel colored by CD34, CD45, CD33, CD15, CD64 intensity (**C**) Percentage of HSPCs (N = 3, Wilcoxon test p-value: 0.03, 0.02 and 0.005 for day 7, day 14 and day 21 respectively) PMNs (N = 3, Wilcoxon test p-value: 0.4, 0.07 and 0.007 for day 7, day 14 and day 21 respectively) and monocytes at the each time point in the AMO (green) and the 2D (blue) model (N = 3, Wilcoxon test p-value: 0.03, 0.0001 and 0.002 for day 7, day 14 and day 21 respectively). (**D**) Colony-forming unit assay of FACS-sorted CD34 + HSPC from AMO after 2 weeks of culture with the myeloid differentiation protocol. CFU-GM, granulocyte-macrophage colony-forming unit; CFU-GEMM, granulocyte, erythrocyte, monocyte, megakaryocyte colony-forming unit. Representative phase contrast microscopy of colonies morphology (right). Scale Bar 200 µm. N = 3. (**E**) Percentage of HSPCs, PMNs, and monocytes after 2 weeks of culture with the myeloid differentiation protocol, in a secondary AMO built with CD34 + HSPCs replated from a primary AMO. (**F**) Morphological evaluation of one representative myeloid cell differentiation at 14 days, observed after MGG staining of cell cytospin recovered from 2D cultures or AMO. One experiment out of three is presented. Orange arrow points to PMNs. Scale bar 60 µm. PMN and monocytes cells count for 3 independent experiments (right panel). (**G**) Histogram of intracellular MPO expression (left) and median fluorescent analysis (MFI, right) on PMN (orange) and monocytes (red) after 14 days of culture with the myeloid differentiation protocol within the AMO.

microenvironment[27]. However, studying these processes *in vivo* presents significant challenges. This is where the innovation in developing appropriate 3D models comes into play. Herein, we illustrated the simplicity of the AMO model to study myeloid and NK cell ontogenesis. Our data suggest that the AMO system better recapitulates aspects of myeloid differentiation compared to a 2D system. This is evidenced by its greater efficiency at producing PMNs and its ability to support the progenitor pool over a longer period, counting in weeks and not in days compared to the conventional culture methods. Multiple factors, such as cytokine gradients, reduced oxygen availability, and cell–cell or cell–matrix interactions, may all play a role in favoring the granulocyte lineage over monocyte differentiation as well as the maintenance of the HSPC population in within the AMO model[5,28–31]. Interestingly, this balance between myeloid cell subsets reflects the human BM tissue infiltrate with both the physiological predominance of granulocytes compared to other white blood cells[32] and the asynchronous entry into the maturation process facilitated by the persistence of progenitors[33].

On the other hand, the AMO fully supported NK cell development and functionality, paving the way for further studies on how NK cells differentiate from progenitor cells, interact with their environment in the BM, and respond to various stimuli during infections, cancer, and immune disorders. In particular, our model is the first one to address the question how the BMM can support, reshape and eventually interfere with the production and function of NK progenitors and mature cells. This is of particular interest while studying aging or age-associated hematological malignancies, in which HSPCs are functionally impaired, exhibit myeloid-biased differentiation, clonal hematopoiesis and reduced NK cell potential[34,35]. Advances in understanding the molecular mechanisms and developing innovative research models hold significant promise for improving the diagnosis, treatment, and management of various hematological disorders.

In parallel of hematopoietic differentiation analysis, the AMO represents a reproducible platform to characterize the stromal cells themselves. Indeed, the use of a high MSC/hematopoietic cell ratio to build the 3D structure reinforces and enhances the interactions between the two cell subsets. By this way, the AMO deliberately focuses on the cell interplay either orchestrated, or reversely endured, by MSCs through the dialogue with hematopoietic partners. Manipulating one of the AMO cell constituents allows to investigate the consequences on the others, including by adding immunomodulating molecules. Our model is intentionally simplified and does not aim to fully replicate the complex morphology of the BM. The primary application of this model could be to investigate the interactions between h-MSCs and hematopoietic cells, as observed in the hematopoietic niche. By utilizing this simplified system, we aim to gain a deeper understanding of the fundamental cellular interactions between h-MSCs and hematopoietic cells, without the additional complexity of other BM cell types. Adding key structural cells, such as osteoblasts, endothelial cells, and adipocytes, to the organoid could provide valuable insights, making it a promising direction for future research.

The AMO protocol offers advantages over the 2D pre-existing systems including (i) a fully human model based on h-MSC which create an *in vivo*–mimicking environment for hematological cells, (ii) the possibility to study different hematological cells changing only the cocktail of cytokines, (iii) the 3D architecture taking into account complex cell-cell interactions and physical constraints, (iv) a more physiological context than 2D cultures for drug screening, including intercellular drug diffusion and molecular accessibility. Nevertheless, at that stage, the AMO share some limitations associated with the 3D *in vitro* system and in particular the lack of other types of stromal cells, of the neuronal system and of a circulation network. Further studies involving the incorporation of other cell types such as additional immune partners, including CD8 + or CD4 + T cells, endothelial cells, or leukemic cells into the AMO, or conducting experiments in an autologous setting, could enhance the reliability and applicability of the model. Meanwhile, the AMO is a straightforward, versatile, reproducible and scalable platform, meeting basic and clinical exigencies.

A Representative plot of flow cytometry analysis

B

C

Week 2 Week 4

- 0.30% HSC
- 2.10% CLP
- 47.90% Stage 3
- 41.30% Stage 4
- 7.00% Stage 5
- 1.40% Stage 6
- 0.10% CLP
- 8.00% Stage 3
- 77.20% Stage 4
- 13.50% Stage 5
- 1.20% Stage 6

D Functional Proteins

CD16, Perforin, Granzyme B

Activating receptors: NKp30, NKp46, DNAM1, NKG2D

Inhibitory receptors: KIR2D, NKG2A

E Polyfunctional assay

Baseline, K562, PMA + ionomycin

- resting cells
- CD107a+ — Monofunction
- IFNg+
- TNFa+
- IFNg+CD107a+ — Bifunction
- TNFa+IFNg+
- TNFa+CD107a+
- TNFa+IFNg+CD107a+ — Trifunction

Altogether, this model provides a powerful tool for studying hematopoiesis, immune responses, and disease mechanisms holding great promise for drug testing and the development of new therapies.

Materials and methods
Primary cells

Bone marrow (BM) samples were obtained from patients, free of hematological disease and coming to the Orthopedic and Trauma surgery Department of Lariboisiere Hospital (Paris, France) for a total hip replacement surgery. Peripheral blood samples were provided from the blood biobank of Saint-Louis Hospital (Paris, France). Cord blood samples were provided by the Cord Blood Biobank, Cell Therapy unit, of Saint-Louis Hospital (authorization AC-2022-5325). All the patients provided written informed consent, in accordance with the Helsinki Declaration. Approval from the Ethics Review Committee for Biomedical Research Projects Paris

◀**Fig. 4**. NK cell differentiation from HSPCs to mature effector cells. (**A**) Gating strategy allowing to distinguish the different stages of NK cell maturation: HSC (CD34 + CD38-), CLP (CD34 + CD38 + CD10 + CD45RA+), immature NK cells (stage 3: CD34- CD45RA + CD56- CD16-), and mature NK cells (stage 4: CD34-CD45RA + CD56bright CD16-, stage 5: CD34- CD45RA + CD56dim CD16 + and stage 6: CD34-CD45RA + CD56dim CD16 + CD57 + KIR2D+/-). Plots at two weeks of differentiation. (**B**) Tree representation of SPADE clustering colored by pseudotime calculated using trajectory analysis with Wishbone algorithm of NK cell differentiation taking CD34 + CD38- HSC population as starting cell type. The size of nodes is proportional to the number of cells in the given cluster. Calculation and figure were made with the OMIQ software (https://www.omiq.ai/). The differentiation stages have been manually added to the figure in base of the expression of main lineage markers. The same SPADE tree is represented in the lower panel colored based on CD34 and CD56 intensity. For other markers, see Supplemental Fig. 2B. (**C**) Evolution of NK cell differentiation stages in percentage at two and four weeks of AMO culture ($N = 2$ at 2 weeks and $N = 3$ at 4 weeks), calculated as percentage of total NK cells using the gating strategy above mentioned. (**D**) Phenotype of a representative AMO after two weeks; plot of live NK cells gated on stage 5 cell subset as defined in (A). The positivity of NK cell receptors is assessed by comparison to unstained cells gated on forward scatter. (**E**) Evaluation of NK cell polyfunctionality after 3 weeks of AMO culture ($N = 4$). After organoid dissociation, NK cells were cultured either in presence of the NK sensitive K562 cell line or with PMA-Ionomycin. NK cell degranulation of cytolytic granules (surface expression of CD107a) and IFN-γ and TNF-α intracellular richness were determined by flow cytometry. Proportion of NK cells with monofunction, bifunction and trifunction significantly increased after stimulation by K562 cell line or PMA and ionomycin (p-value of 0.02 and < 0.01 for K562 and PMA-Ionomycin versus control respectively, Fisher exact test).

Nord (CEERB, IRB #00006477) was obtained before the use of the clinical materials for research purposes. Mononuclear cells were purified from the BM or blood samples with a Ficoll gradient (Pancoll Human, PAN-BIOTECH). Human CD34 + cells were magnetically enriched with the EasySep™ Human CD34 Positive Selection Kit II (STEMCELL Technologies) from either BM or CB samples. In the same way, mature NK cells were isolated from peripheral blood mononucleated cells with the EasySep™ Human NK Cell Enrichment Kit (STEMCELL Technologies). Human mesenchymal stromal cells (h-MSC) were derived from BM samples and separated from other hematopoietic cells through their plastic adherence after 2–3 weeks of *in vitro* culture. H-MSC were then expanded in αMEM (Gibco) supplemented with 10% fetal bovine serum (FBS, Sigma), 2 mM glutamine, 100 U/mL penicillin and 100 µg/mL streptomycin (Gibco). When the h-MSC reached 80–90% confluence, the cells were detached with Trypsin (Gibco) and cryopreserved before use. Four different h-MSCs were used in this study. The donor individuals have a median age of 70 years (range: 59–80), including two males and two females. All the MSCs were used between passages 2 to 4.

Artificial marrow organoid (AMO) culture

The 3D culture was adapted from *Seet at al*[18]. In details, h-MSC were harvested by trypsinization and resuspended in serum-free culture medium, so-called AMO medium, composed of RPMI 1640 (Gibco), 4% B27 supplement (ThermoFisher Scientific), 30 µM L-ascorbic acid 2-phosphate sesquimagnesium salt hydrate (Sigma) reconstituted in PBS, 100 U/mL penicillin and 100 µg/mL streptomycin (Gibco), 2 mM glutamine (ThermoFisher Scientific) and a specific cocktail of cytokines depending on the experiments and constituted as follows: myeloid differentiation cytokine cocktail (based on *Sakuraii et al.*[36]): IL-3 7 ng/mL (Miltenyi), SCF 100 ng/mL (Miltenyi), TPO 10 ng/mL (Miltenyi), FLT3-L 200 ng/mL (Miltenyi); NK differentiation cytokine cocktail (based on *Freud et al.*[37,38]). : IL-7 10 ng/mL (Miltenyi), SCF 10 ng/mL (Miltenyi), TPO 10 ng/mL (Miltenyi), FLT3-L 10 ng/mL (Miltenyi), IL-15 20 ng/mL (Miltenyi), SR-1 2 µM (Miltenyi); NK stimulation cocktail: IL-2 100 UI/mL (Miltenyi). Depending on the experiment, 8×10^4 to 1.5×10^5 h-MSCs were combined with 6×10^3–7.5×10^3 purified CD34 + cells or 4×10^4 NK cells per AMO in 1.5 ml Eppendorf tubes and centrifuged at 300 g for 5 min. Supernatants were carefully removed and the cell pellets were harvested. For each AMO, a 0.4 µm Millicell transwell insert (EMD Millipore) was placed in a 6-well plate containing 1 mL of AMO medium per well supplemented with the appropriate cytokines. Medium was fully changed every 3 days. The AMO were kept in culture for different time points depending on the experiments: up to 3 weeks for the myeloid maturation, for 4 weeks for the NK ontogenesis, and for 1 to 7 days for the NK functional experiments. At the indicated time points, AMOs were harvested and dissociated with collagenase (Thermofisher) at a final concentration of 200 U/mL in 1X PBS for 30 min at 37 °C. When the analyses on the MSC compartment is not required a passage through a 50 µm nylon strainer is recommended.

2D cell culture

H-MSCs were seeded overnight on 24 or 6 wells plates in normal α-MEM supplemented with 10% fetal bovine serum (FBS, Sigma), 2 mM glutamine, 100 U/mL penicillin and 100 µg/mL streptomycin (Gibco). The day after, the media was removed and the CD34 + cells were added to the culture conditions (at the same ratio used in the AMO culture). The co-cultures were maintained in the same AMO medium and analyzed in parallel of the 3D systems.

H-MSC differentiation

To compare the differentiation and clonogenic capacities of FACS sorted h-MSC after 3D culture or *ex-vivo* expanded MSC culture, CFU-F (colony forming units-fibroblast), adipogenic and osteogenic differentiations were performed as described elsewhere[39]. Briefly, for CFU-F, 200 h-MSCs were distributed in 25 cm² flask in
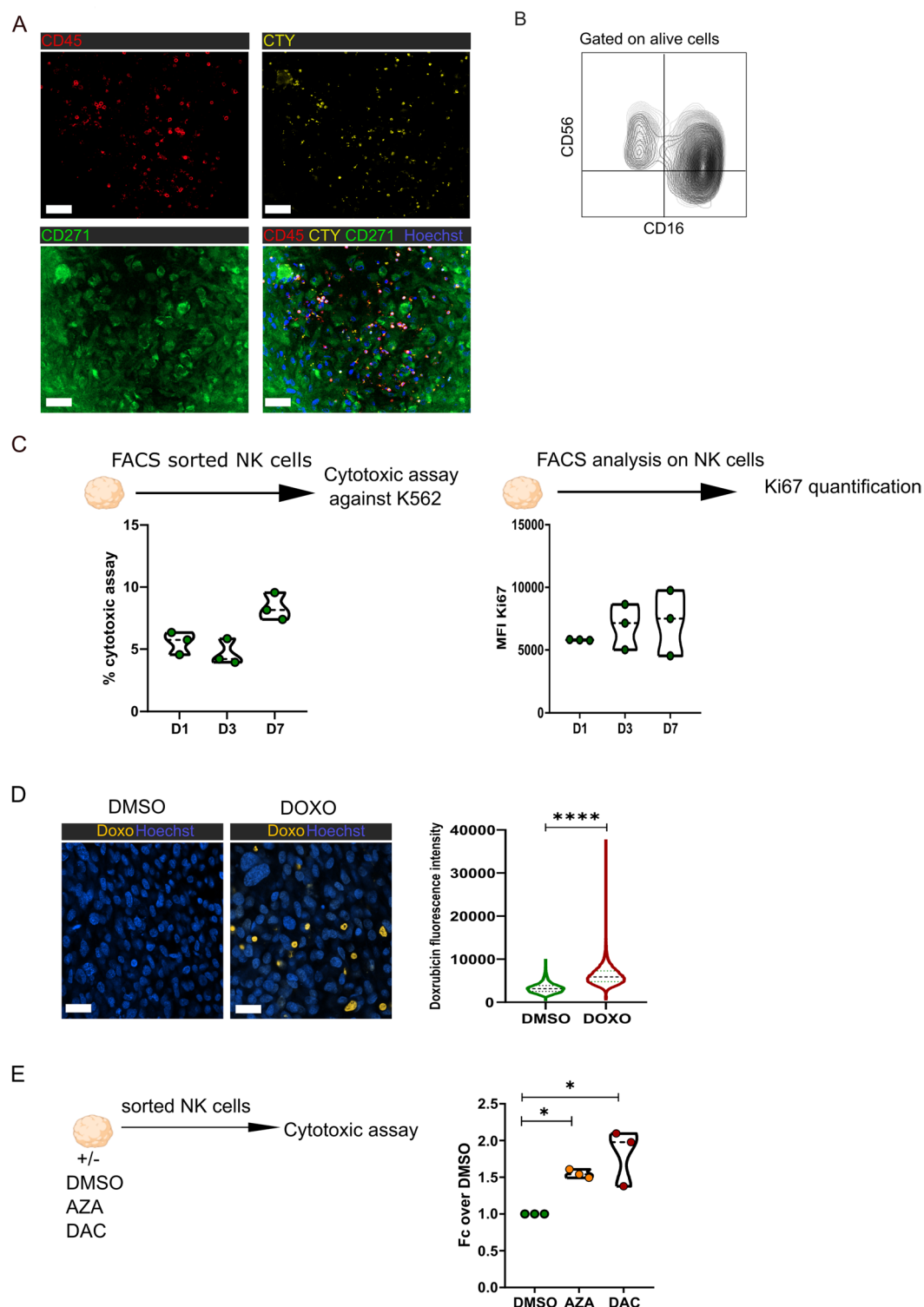
7mL of complete α-MEM FBS medium for three weeks with a medium change once a week. 5.000 h-MSCs were distributed in 24-well plates for osteogenic and adipogenic differentiation for 21 days. After 24 h of adhesion, the osteogenic or adipogenic media were added onto the induced wells, whereas complete α-MEM FBS medium or adipogenic maintenance medium was added onto the control wells. At the end of the experiments, medium was removed, cells were fixed and stained following fabricant's recommendations with 2% crystal violet (SIGMA), 2% red alizarin (SIGMA) or oil red (Lipid oil red staining kit, SIGMA) to assess CFU-F, osteogenic and adipogenic differentiation, respectively (Fig. 1E-G).

CD34 + CFU and replating assay

To determine the differentiation ability and stemness of AMO-derived HSPCs, a CFU assay was conducted with FACS-sorted CD34 + cells. The assay was performed in duplicate. Briefly, sorted cells were diluted in

◀**Fig. 5**. Drug testing. (**A**) Confocal imaging of NK cell infiltration in a representative AMO after staining with Hoechst (nuclei, blue), CD271-AF488 (h-MSC, green), CellTrace Yellow (CTY; NK cell, yellow) and CD45-AF647 (NK cell, red). Scale bar 50 μm. (**B**) Lineage markers (CD56 and CD16) representation of spectral flow-cytometry analysis performed on NK cells from the same donor co-cultured for three days with h-MSC ($N = 3$) in AMO cultures. (**C**) Overtime assessment of cytotoxic function and cell proliferation on the NK cells after AMO co-culture. Cytotoxicity against K562 cell line (measure of calcein release by fluorescence and expressed in percentage of specific lysis based on spontaneous and maximum release, left panel) and Ki67 marker (right panel). Data are represented as mean ± SD. (**D**) Confocal imaging and quantification and imaging on the AMO model after treatment with doxorubicin (10μM for two hours) vs. control (DMSO). Hoechst in blue and Doxorubicin in yellow. Scale bar 20 μm. ($N = 3$, Wilcoxon test p-value < 0,0001). Data are represented as mean ± SD. (**E**) Quantification of the cytotoxic activity measured by calcein-release by K562 cell line in presence of NK cells co-cultured in AMO in presence of AZA or DAC for three days ($N = 3$, Mann Whitney test p-value < 0,05). Data are represented as mean ± SD.

RPMI (Gibco) medium containing 1% penicillin-streptomycin and then added to complete MethoCult H4435 enriched medium (STEMCELL Technologies). A total of 1,000 cells were seeded per 19 mm dish, and CFUs were counted on day 14 using a light microscope. For the replating experiments, a secondary passage was performed in organoids with 6×10^3 FACS-sorted CD34 + cells. The myeloid differentiation protocol mentioned above was followed.

NK cell functional assays

NK cell cytotoxicity was assessed thanks to a calcein release assay[40,41]. Briefly, in this assay Calcein-AM (Calcein acetoxymethyl ester), a non-fluorescent compound, is utilized to label target cells. Once taken up by the cells, Calcein-AM is converted into its fluorescent form by intracellular esterases, resulting in the retention of a bright fluorescence signal within live cells. K562, a human NK-sensitive erythroleukemia cell line, was used as target cell. The K562 cell line was labeled with 1 μg/mL calcein (ThermoFisher Scientific) in PBS for 1 h at 37°C. NK cells were dissociated from the AMO after 3 days of culture, enumerated and co-cultured with calcein-labeled K562 cells in 96-well U-bottom plates in a medium supplemented with Probenecid at 1:1 effector: target ratio. The killing was quantified after 4 h of incubation at 37 °C by measuring calcein-release into the supernatant (BMG CLARIOstar microplate reader). During this time, if NK cells effectively kill the K562 cells, the cell membrane integrity of the K562 cells is compromised, leading to the release of Calcein from the cells into the surrounding medium which can be measured using a fluorescence plate reader. A high cytotoxicity response is indicated by a significant increase in fluorescence within the media, suggesting that the NK cells are efficiently killing the K562 cells. Conversely, low cytotoxicity is reflected by minimal or no fluorescent signal, indicating that the NK cells are not effectively killing the target cells. The specific killing was calculated using the following formula: (Experimental fluorescence of K562 + NK cell well—Spontaneous fluorescence)/(Maximum fluorescence—Spontaneous fluorescence); where spontaneous fluorescence refers to the baseline fluorescence signal from live K562 cells, and maximum fluorescence represents the highest signal obtained from fully lysed K562 cells. For the IFN-γ and TNF-α quantification, enriched NK cells were cultured with PMA-Ionomycin (SIGMA, 50 and 500 ng/mL, respectively) or K562 cells (1:1 effector: target ratio) for 5 h at 37 °C. Brefeldin A (Sigma) was added at a final concentration of 10 μg/ml after 1 h of incubation. The percentage of CD107a, IFN-γ and TNF-α positive cells was estimated by flow cytometry in the CD3 − CD56 + NK cells. Spontaneous release was detected in the absence of target cells.

Flow-cytometry analysis

After AMO dissociation, cells were washed in PBS and stained with the antibodies presented in Supplemental Table 2 acquired on Aurora (Cytek®). For intracellular staining the eBioscience™ Foxp3/Transcription Factor Staining Buffer Set (ThermoFisher) was used. Supervised analyses were performed on data extracted from FlowJo v10.7 software and analyzed with GraphPad Prism v8.0 software. Uniform manifold approximation and projection (UMAP) and trajectory analyses using wishbone algorithm were performed with OMIQ software from Dotmatics (https://www.omiq.ai, analysis performed with the online version available between January 2024 to March 2025, © 2025 Dotmatics, https://wwwdotmatics.com).

Staining and microscopy

The AMO were fixed, without prior dissociation, with 4% paraformaldehyde (PFA, Sigma) for 15 min and permeabilized with 0.3% Triton-X-100 (Sigma) in PBS for 15 min. Blocking solution (0.5% BSA in PBS) was then used for at least 1 h. After the blocking step, the AlexaFluor647-labeled CD45-specific monoclonal antibody (Biolegend), anti-CD271 (NGFR, Sigma) and the TRITC-labeled Phalloidin (Sigma) were used in a solution with saponin 0.025% in PBS, and incubated with the AMO overnight at 4°C. NK cells were stained with CellTrace™ Yellow (ThermoFisher) according to the manufacturer´s protocol prior to AMO building. Images were acquired by laser scanning microscopy on a LSM 800 AiryScan system mounted on an Axio Observer stand (Zeiss, Oberkochen, Germany) and with a Plan Apochromat 63X N.A. 1.4 oil-immersion objective using the Zen Blue edition software (Zeiss, v2.3). The pixel size was set at 0.71 μm and a z-step of 0.5 μm was used. The quantification of AMO diameters, the CD45+ cell distance and fluorescence intensity (CD45-AF647 and doxorubicin) were performed using QuPath software (v0.5.0). May Grunwald Giemsa (MGG) staining was performed on cells harvested, sorted and cytospined after AMO co-culture with myeloid differentiation

induction. Different stages of the myeloid differentiation were morphologically identified by optical microscopy and counted over a total of 200 cells.

In vitro cell treatment and functional assay

The AMOs were treated with doxorubicin (DOXO), a chemotherapeutic drug with autofluorescence property[22] (excitation 480–500 nm/emission 590 nm) at a specific concentration (10 μm) and time point (2 h). After doxorubicin treatment, the AMOs were fixed with 4% PFA, stained with Hoechst, and imaged under a microscope. AMO were treated in AMO cell culture medium with 0.5 μM of AZA or DAC (Sigma). DMSO only was used as control. The treatments were maintained for 3 days with a half change of medium after 48 h (IL-2 + drugs or DMSO). Then, cells were collected and NK cells were analyzed for their cytotoxic capacity as described above.

Statistical analyses

Data were expressed as the mean ± standard deviation of means from the indicated number of experiments. To test differences between groups Mann-Whitney or Wilcoxon test was used. Statistical significance was considered at p-value < 0.05 utilizing prism (Graphpad).

Data availability

The datasets used and/or analyzed during the current study available from the corresponding author on reasonable request.

References

1. Lang, Y., Lyu, Y., Tan, Y. & Hu, Z. Progress in construction of mouse models to investigate the pathogenesis and immune therapy of human hematological malignancy. *Front. Immunol.* **14**, 1195194 (2023).
2. Sommerkamp, P., Mercier, F. E., Wilkinson, A. C., Bonnet, D. & Bourgine, P. E. Engineering human hematopoietic environments through ossicle and bioreactor technologies exploitation. *Exp. Hematol.* **94**, 20–25 (2021).
3. Pievani, A. et al. Harnessing mesenchymal stromal cells for the engineering of human hematopoietic niches. *Front. Immunol.* **12** (2021).
4. Unnikrishnan, K., Thomas, L. V. & Ram Kumar, R. M. Advancement of Scaffold-Based 3D cellular models in Cancer tissue engineering: an update. *Front. Oncol.* **11** (2021).
5. de Janon, A., Mantalaris, A. & Panoskaltsis, N. Three-Dimensional human bone marrow organoids for the study and application of normal and abnormal hematoimmunopoiesis. *J. Immunol.* **210**, 895–904 (2023).
6. Eaves, C. J. Hematopoietic stem cells: concepts, definitions, and the new reality. *Blood* **125**, 2605–2613 (2015).
7. Vo, L. T. & Daley, G. Q. De Novo generation of HSCs from somatic and pluripotent stem cell sources. *Blood* **125**, 2641–2648 (2015).
8. De Kleer, I., Willems, F., Lambrecht, B. & Goriely, S. Ontogeny of myeloid cells. *Front. Immunol.* **5** (2014).
9. Rosenbauer, F. & Tenen, D. G. Transcription factors in myeloid development: balancing differentiation with transformation. *Nat. Rev. Immunol.* **7**, 105–117 (2007).
10. Fine, N., Tasevski, N., McCulloch, C. A., Tenenbaum, H. C. & Glogauer, M. The neutrophil: constant defender and first responder. *Front. Immunol.* **11** (2020).
11. Kondo, M. et al. Cell-fate conversion of lymphoid-committed progenitors by instructive actions of cytokines. *Nature* **407**, 383–386 (2000).
12. Kyrysyuk, O. & Wucherpfennig, K. W. Designing Cancer immunotherapies that engage T cells and NK cells. *Annu. Rev. Immunol.* **41**, 17–38 (2023).
13. Vivier, E. et al. Natural killer cell therapies. *Nature* **626**, 727–736 (2024).
14. Lanier, L. L. Five decades of natural killer cell discovery. *J. Exp. Med.* **221**, e20231222 (2024).
15. Granzin, M. et al. Shaping of natural killer cell antitumor activity by ex vivo cultivation. *Front. Immunol.* **8** (2017).
16. Roeven, M. W. H. et al. The Aryl hydrocarbon receptor antagonist stemRegenin1 improves in vitro generation of highly functional natural killer cells from CD34 + Hematopoietic stem and progenitor cells. *Stem Cells Dev.* **24**, 2886–2898 (2015).
17. Cany, J. et al. Combined IL-15 and IL-12 drives the generation of CD34+-derived natural killer cells with superior maturation and alloreactivity potential following adoptive transfer. *OncoImmunology* **4**, e1017701 (2015).
18. Seet, C. S. et al. Generation of mature T cells from human hematopoietic stem and progenitor cells in artificial thymic organoids. *Nat. Methods.* **14**, 521–530 (2017).
19. Blanco, T. M., Mantalaris, A., Bismarck, A. & Panoskaltsis, N. The development of a three-dimensional scaffold for *ex vivo* biomimicry of human acute myeloid leukaemia. *Biomaterials* **31**, 2243–2251 (2010).
20. Syrjälä, M., Ruutu, T. & Jansson, S. E. A flow cytometric assay of CD34-positive cell populations in the bone marrow. *Br. J. Haematol.* **88**, 679–684 (1994).
21. Di Vito, C., Mikulak, J. & Mavilio, D. On the way to become a natural killer cell. *Front. Immunol.* **10** (2019).
22. Shah, S. et al. Fluorescence properties of doxorubicin in PBS buffer and PVA films. *J. Photochem. Photobiol B.* **170**, 65–69 (2017).
23. Sohlberg, E. et al. Imprint of 5-azacytidine on the natural killer cell repertoire during systemic treatment for high-risk myelodysplastic syndrome. *Oncotarget* **6**, 34178–34190 (2015).
24. Boy, M. et al. Myelodysplastic syndrome associated TET2 mutations affect NK cell function and genome methylation. *Nat. Commun.* **14**, 588 (2023).
25. Boulais, P. E. & Frenette, P. S. Making sense of hematopoietic stem cell niches. *Blood* **125**, 2621–2629 (2015).
26. Soto, C. A., Celso, L., Purton, C., Frisch, B. J. & L. E. & From the niche to malignant hematopoiesis and back: reciprocal interactions between leukemia and the bone marrow microenvironment. *JBMR Plus.* **5**, e10516 (2021).
27. Restelli, C. et al. Recent advances in Immune-Based therapies for acute myeloid leukemia. *Blood Cancer Discov.* **5**, 234–248 (2024).
28. Peshkova, M. et al. MSCs' conditioned media cytokine and growth factor profiles and their impact on macrophage polarization. *Stem Cell. Res. Ther.* **14**, 142 (2023).
29. Ropa, J. et al. Local oxygen dictates hematopoietic cell growth and function. *Blood* **142**, 1307 (2023).
30. Jing, D. et al. Oxygen tension plays a critical role in the hematopoietic microenvironment in vitro. *Haematologica* **97**, 331–339 (2012).
31. Sangaletti, S., Chiodoni, C., Tripodo, C. & Colombo, M. P. Common extracellular matrix regulation of myeloid cell activity in the bone marrow and tumor microenvironments. *Cancer Immunol. Immunother CII.* **66**, 1059–1067 (2017).

32. Amulic, B., Cazalet, C., Hayes, G. L., Metzler, K. D. & Zychlinsky, A. Neutrophil function: from mechanisms to disease. *Annu. Rev. Immunol.* **30**, 459–489 (2012).
33. Dussiau, C. et al. Hematopoietic differentiation is characterized by a transient peak of entropy at a single-cell level. *BMC Biol.* **20**, 60 (2022).
34. Chung, S. S. & Park, C. Y. Aging, hematopoiesis, and the myelodysplastic syndromes. *Hematol. Am. Soc. Hematol. Educ. Program.* **2017**, 73–78 (2017).
35. Qi, C. & Liu, Q. Natural killer cells in aging and age-related diseases. *Neurobiol. Dis.* **183**, 106156 (2023).
36. Sakurai, M., Ishitsuka, K., Becker, H. J. & Yamazaki, S. Ex vivo expansion of human hematopoietic stem cells and clinical applications. *Cancer Sci.* **115**, 698–705 (2024).
37. Freud, A. G. et al. NKp80 defines a critical step during human natural killer cell development. *Cell. Rep.* **16**, 379–391 (2016).
38. Freud, A. G. et al. A human CD34(+) subset resides in lymph nodes and differentiates into CD56bright natural killer cells. *Immunity* **22**, 295–304 (2005).
39. Bisio, V., Espéli, M., Balabanian, K., Anginot, A. & Culture Expansion and differentiation of human bone marrow stromal cells. *Methods Mol. Biol. Clifton NJ.* **2308**, 3–20 (2021).
40. Lorenzo-Herrero, S., Sordo-Bahamonde, C., González, S. & López-Soto, A. Chapter Twenty-Six - Evaluation of NK cell cytotoxic activity against malignant cells by the calcein assay. in Methods in Enzymology (eds Galluzzi, L. & Rudqvist) N.-P.) vol. 631 483–495 (Academic, 2020).
41. Rocca, Y. S. et al. Phenotypic and functional dysregulated blood NK cells in colorectal cancer patients can be activated by cetuximab plus IL-2 or IL-15. *Front. Immunol.* **7**, 413 (2016).

Acknowledgements

Author contributions

BS, LPZ, ND and VB designed, analyzed and interpreted all experiments, and wrote the manuscript. BS, LPZ, IM, CK, EL, and VB performed experiments. MK analyzed microscopy experiments. PF, LA, AT, ME and KB contributed to the scientific orientation of the study and critically reviewed the manuscript. CK, AT and EC contributed to the design of the experimental model. ND and VB supervised the study.

Declarations

Competing interests

Bérénice SCHELL, Lin-Pierre ZHAO, Antoine TOUBERT, Marion ESPELI, Karl BALABANIAN, Nicolas DULPHY, Valeria BISIO and the French National Institute of Health and Medical Research (INSERM) declare pending patent application (#EP23306658.8) relating to the AMO system. All other authors have no competing interest.

Additional information

Supplementary Information The online version contains supplementary material available at https://doi.org/10.1038/s41598-025-07717-9.

Correspondence and requests for materials should be addressed to N.D. or V.B.

Reprints and permissions information is available at www.nature.com/reprints.

Publisher's note Springer Nature remains neutral with regard to jurisdictional claims in published maps and institutional affiliations.